Articles

Crystal Structures of a Low-Molecular Weight Protein Tyrosine Phosphatase from *Saccharomyces cerevisiae* and Its Complex with the Substrate *p*-Nitrophenyl Phosphate[†,‡]

Shuishu Wang,[§] Lydia Tabernero,[||,⊥] Marie Zhang,[§,@] Etti Harms,[||] Robert L. Van Etten,[§] and Cynthia V. Stauffacher*[,||]

Departments of Chemistry and Biological Sciences, Purdue University, West Lafayette, Indiana 47907

Received June 11, 1999; Revised Manuscript Received November 18, 1999

ABSTRACT: Low-molecular weight protein tyrosine phosphatases are virtually ubiquitous, which implies that they have important cellular functions. We present here the 2.2 Å resolution X-ray crystallographic structure of wild-type LTP1, a low-molecular weight protein tyrosine phosphatase from *Saccharomyces cerevisiae*. We also present the structure of an inactive mutant substrate complex of LTP1 with *p*-nitrophenyl phosphate (*p*NPP) at a resolution of 1.7 Å. The crystal structures of the wild-type protein and of the inactive mutant both have two molecules per asymmetric unit. The wild-type protein crystal was grown in HEPES buffer, a sulfonate anion that resembles the phosphate substrate, and a HEPES molecule was found with nearly full occupancy in the active site. Although the fold of LTP1 resembles that of its bovine counterpart BPTP, there are significant changes around the active site that explain differences in their kinetic behavior. In the crystal of the inactive mutant of LTP1, one molecule has a *p*NPP in the active site, while the other has a phosphate ion. The aromatic residues lining the walls of the active site cavity exhibit large relative movements between the two molecules. The phosphate groups present in the structures of the mutant protein bind more deeply in the active site (that is, closer to the position of nucleophilic cysteine side chain) than does the sulfonate group of the HEPES molecule in the wild-type structure. This further confirms the important role of the phosphate-binding loop in stabilizing the deep binding position of the phosphate group, thus helping to bring the phosphate close to the thiolate anion of nucleophilic cysteine, and facilitating the formation of the phosphoenzyme intermediate.

Protein phosphorylation and dephosphorylation on tyrosine residues by kinases and phosphatases play an important role in cellular regulation and signal transduction (*1*, *2*). The importance of the protein tyrosine phosphatases (PTPases)[1] in cellular signaling processes is now increasingly recognized (*3*−*5*). PTPases can be divided into three major families based on their size and substrate specificity: the high-molecular weight PTPases, the dual specificity PTPases, and the low-molecular weight PTPases (*6*). Despite the fact that there is little sequence similarity among these families of PTPases, they share a common active site signature motif, CXXXXXRS/T (single-letter amino acid codes).

The high-molecular weight PTPase family includes receptor and nonreceptor PTPases. These PTPases have a conserved ∼30 kDa catalytic domain, and share a high degree of sequence and structural homology (*7*−*10*). The active site cavity is deep and hydrophobic, allowing only phosphotyrosine to enter and to be dephosphorylated. In contrast, dual specificity PTPases have a shallower active site, allowing for the hydrolysis of phosphorylated serine and threonine residues, in addition to phosphotyrosine (*11*). The crystal structure of a dual specificity PTPase, VHR (*12*), reveals an overall structure that resembles that of the catalytic domain of high-molecular weight PTPases. In contrast to

[†] This research was supported by American Cancer Society Grant NP-946 awarded to C.V.S. and by United States Department of Health and Human Services Research Grant GM 27003 to R.L.V.E. and CA 82673 to C.V.S. Data collection facilities were supported in part by an NCI grant to the Purdue Cancer Center.

[‡] The atomic coordinates of the wild-type LTP1 and of the LTP1−C13A mutant complexed with *p*NPP have been deposited with the Protein Data Bank under file names 1D1P and 1D1Q, respectively.

* To whom correspondence should be addressed. Fax: (765) 496-1189. E-mail: cyndy@gauguin.bio.purdue.edu.

[§] Department of Chemistry.

[||] Department of Biological Sciences.

[⊥] Current address: School of Biological Sciences, University of Manchester, 2.205 Stopford Bldg., Oxford Road, Manchester M139PT, U.K.

[@] Current address: 3-Dimensional Pharmaceuticals, Inc., Eagleview Corporate Center, Suite 104, 665 Stockton Dr., Exton, PA 19341.

[1] Abbreviations: PTPase, protein tyrosine phosphatase; low-M_r PTPase, low-molecular weight protein tyrosine phosphatase; BPTP, bovine low-M_r protein tyrosine phosphatase; LTP1, low-M_r PTPase from *Saccharomyces cerevisiae*; STP1, low-M_r PTPase from *Schizosaccharomyces pombe*; VHR, vaccinia H1-related dual specificity phosphatase; *p*NPP, *p*-nitrophenyl phosphate; HEPES, *N*-(2-hydroxyethyl)piperazine-*N*′-2-ethanesulfonic acid; Bis-Tris, bis(2-hydroxyethyl)iminotris(hydroxymethyl)methane; FMN, flavin mononucleotide; DEM, diethylmalonic acid; rms, root-mean-square.

10.1021/bi991348d CCC: $19.00
Published on Web 02/03/2000

what appears to be a conservation of domain structure for phosphatase activity, the recently determined structure of cdc25A has a different fold that resembles that of rodanese (*13*), and may represent another phosphatase family.

The low-molecular weight protein tyrosine phosphatases (low-M_r PTPases) are single-domain cytosolic enzymes with molecular masses of approximately 18 kDa. The active site sequence motif of these enzymes is located near the N-terminus, and has a conserved (V/I)CXGNXCRS sequence. Members of this family of PTPases have been identified in a wide variety of organisms, including bacteria, yeast, rat, bovine, and human (*14*−*20*). This broad distribution suggests that these enzymes have important cellular functions, and many potential substrates have been suggested. A recent study on Eph receptors (*21*) suggests that in vertebrates, the low-M_r PTPases are involved in the ephrin signaling pathway. Yeast serves as a simple, but often useful, model system for studying the biological function of many kinases and PTPases. Two low-M_r PTPases from yeast have been cloned, namely, LTP1 from *Saccharomyces cerevisiae* (*15*) and STP1 from *Schizosaccharomyces pombe* (*20*). The sequences of both enzymes are relatively similar to the mammalian low-M_r PTPases, 42 and 39% for the STP1 and LTP1, respectively. The gene for STP1 was cloned as a multicopy suppressor of a mutation in the cdc25$^+$ gene that encodes a dual specificity phosphatase involved in mitotic control (*22*), indicating its function as a PTPase in the cell. The gene for LTP1 was cloned by low-stringency hybridization using an oligonucleotide probe derived from the active site sequence of the mammalian low-M_r PTPases (*15*).

All the PTPases appear to catalyze the dephosphorylation of substrates by a common mechanism. The conserved active site sequence motif (CXXXXXRS/T) forms a phosphate-binding loop (also called the P-loop), with the side chain of the arginine residue and the backbone NHs of the P-loop hydrogen bonded to the phosphate group of the substrate. The first cysteine in the signature motif functions as a nucleophile, leading to the formation of a phosphoenzyme intermediate (*23*). The nucleophilic cysteine has a pK_a that is much lower than that of the free cysteine. The pK_a values of the nucleophilic cysteine in *Yersinia* PTPase, PTP1B, and VHR have been estimated to be 4.7, 5.4, and 5.6, respectively (*24*−*26*). The pK_a of the low-M_r PTPase BPTP has been estimated to be below 4.0 (*27*). Cysteine residues as thiolate ions (S^-) are much more potent nucleophiles than the corresponding thiol (−SH) form. The thiolate anion is stabilized by hydrogen bonding to the side chain of the conserved serine residue (threonine in some PTPases) (*6*, *27*, *28*), and by the microdipoles generated by the partial charges of the backbone NHs of the P-loop and charge interaction with the side chain of the conserved arginine (*16*, *29*; V. Dillet, R. L. Van Etten, and D. Bashford, unpublished results).

Among the low-M_r PTPases, most of the kinetic and structural studies have focused on the mammalian enzymes. These enzymes are highly homologous, and their sequences are about 85−95% identical. Crystal structures of two members of this family, BPTP and HCPTPA, and an NMR solution structure of BPTP have been obtained (*30*−*33*). Kinetic experiments show that LTP1 has a substrate specificity that is similar but not identical to that of the homologous mammalian enzymes (*15*). However, the catalytic activity of LTP1 toward a number of substrates is approximately 30-fold lower than that for the bovine enzyme BPTP. This relatively low activity can be substantially activated by the presence of adenine and some purine nucleosides and nucleotides (*15*). It was therefore of interest to determine the structure of a yeast enzyme, more distantly related than the bovine and human forms, and to examine the structural differences between the mammalian and yeast enzymes in relation to differences in their kinetic behavior. This work contains the X-ray crystallographic structure of wild-type LTP1 at a resolution of 2.2 Å. We also present a 1.7 Å structure of an inactive mutant in complex with the substrate *p*NPP, the first crystal structure of a substrate complex of the low-M_r PTPase family. The structure of LTP1 is discussed in terms of differences in the kinetic behavior between this yeast enzyme and its mammalian counterparts. An analysis of the substrate complex further confirms the importance of the rigid P-loop structure, and reveals important roles for the residues lining the walls of the active site cavity in substrate binding and recognition.

EXPERIMENTAL PROCEDURES

Subcloning, Expression, and Purification of LTP1. The cloning, expression, and purification of wild-type LTP1 were as described by Ostanin et al. (*15*). Approximately 20 mg of purified protein was obtained from 2 L of culture. On the basis of SDS−PAGE analysis, the protein was more than 95% pure.

Mutant Preparation. Mutations within the ltp1 gene were generated by site specific mutagenesis following the procedure of Vandeyar et al. (*34*). An 850 bp *Bgl*II−*Pst*I restriction fragment containing the wild-type ltp1 gene was transferred from a pT7-7 plasmid into the *Bam*HI−*Pst*I sites of bacteriophage M13mp19. Mutagenic primers 5′-AAAGATATCGGTCGCATTCATTTCATTGGG-3′ and 5′-AAAGATATCGGTCGCATTCATTGCATTGGG-3′ were used for the replacement of cysteine at position 13 with serine and alanine, respectively. To facilitate mutant screening, both primers carried base changes that would create silent mutations resulting in an *Eco*RV restriction recognition site. Mutagenesis was performed using the T7 in vitro mutagenesis kit from United States Biochemical Corp. DNA samples from the resulting plaques were tested for the additional *Eco*RV site. The mutant DNA was digested with the enzymes *Nde*I and *Bam*HI, and the 500 bp fragment containing the mutant ltp1 gene was inserted into the corresponding sites of the expression vector pET23a. The *Escherichia coli* B strain BL21(DE3) was transformed with these recombinant plasmids for overexpression of the mutant LTP1 protein tyrosine phosphatase. The complete nucleotide sequences of the mutant ltp1 genes in the final plasmid constructs were determined to verify the mutation as well as the integrity of the remainder of the gene.

Mutant protein purification followed procedures similar to those for the wild-type enzyme (*15*). After the cells were harvested by centrifugation, they were washed in 10 mM NaOAc (pH 4.8), 1 mM EDTA buffer, and lysed in the same buffer by being passed twice through a French press. The cell debris was spun down, and the supernatant was loaded onto a C-50 Sephadex cation exchange column equilibrated with 10 mM NaOAc (pH 4.8), 1 mM EDTA buffer. The

column was then washed with the same buffer, and eluted with 300 mM sodium phosphate (pH 5.1). The fractions containing the target protein were combined and concentrated, and then run through a G-50 gel filtration column equilibrated with 30 mM sodium phosphate, 10 mM NaOAc (pH 5.0), and 1 mM EDTA. The C13A mutant overexpressed well, and gave more than 30 mg of pure protein from 1 L of cell culture. However, the C13S mutant was expressed very poorly. No C13S enzyme was isolated in purification trials following the same procedures that were used for C13A.

Protein Activity Assays and Kinetic Measurements. Protein activity was assayed in 100 mM NaOAc buffer (pH 5.0), with 1 mM EDTA and an ionic strength of 150 mM adjusted by adding NaCl. The reaction rate was determined by measuring the rate of release of inorganic phosphate using a malachite green assay procedure (*35*) or by monitoring the release of *p*-nitrophenolate by measuring the absorbance at a wavelength of 405 nm as described by Davis et al. (*36*). Competitive inhibition measurements were taken with the use of *p*NPP as a substrate (*37*).

Protein Crystallization. The purified protein was desalted by running through a 10 mL G-25 column with distilled water or low-ionic strength buffer, or by concentrating and diluting with low-ionic strength buffer three or four times. The desalted protein was further concentrated to a final concentration of approximately 10 mg/mL. Crystallization experiments were carried out using the sitting drop vapor diffusion method. In each drop, 5 μL of protein solution was mixed with 5 μL of well buffer. Wild-type enzyme crystals were obtained from drops set up with a well buffer of 12−18% PEG 3400 and 100 mM NaCl in 100 mM HEPES (pH 7.0) at room temperature. These crystals were very thin plates with dimensions of about 0.05 mm × 0.1 mm × 0.25 mm. For the mutant C13A protein, cocrystallization with substrates was performed in Bis-Tris buffer (pH 7.0) in place of HEPES buffer, because the sulfonate competes with the substrate for binding at the active site (*37*). Crystals were obtained in 13−22% PEG 3400 and 50 mM NaCl in 100 mM Bis-Tris buffer (pH 7.0), with 20 mM *p*NPP at 20 °C. The crystals grew in about 1 week, and the dimensions of the largest crystals were approximately 0.2 mm × 0.5 mm × 1 mm.

Structure Determination. X-ray diffraction data were collected on an R-Axis II or an R-Axis IV imaging plate system (Molecular Structure Corp.) mounted on a Rigaku RU200 rotating anode X-ray generator operating at 50 kV and 100 mA. The wild-type protein data set was collected at room temperature from two crystals obtained in the same batch of crystallization experiments. These crystals diffracted strongly up to a resolution of 2.2 Å. Mutant protein data were collected from a single crystal under cryogenic conditions at approximately −150 °C. The cryogenic solvent that was used was the crystallization mother liquor with 16% glycerol added. The crystals were first soaked in the mother liquor with 1% glycerol. The concentration of glycerol was then gradually increased by removing the solution and adding new solution with increasing glycerol concentrations. The mutant protein crystals diffracted to approximately 1.6 Å resolution, and the data were processed up to 1.7 Å. The data completeness at the last resolution bin is low due to the fact that the diffraction spots were collected in the corners of the image plates.

Table 1: Data Processing Statistics for the LTP1 Crystals

	wild type	C13A and *p*NPP
space group	$P2_12_12_1$	$P2_12_12_1$
cell parameters	$a = 41.6$ Å	$a = 45.9$ Å
	$b = 67.7$ Å	$b = 64.2$ Å
	$c = 115.2$ Å	$c = 112.0$ Å
temperature for data collection	room temperature	cryotemperature (−150 °C)
resolution range (Å)	30−2.2	30−1.7
no. of unique reflections (no. of total observations)	15614 (140622)	32773 (240634)
completeness (%) (last bin completeness)[a]	91.1 (84.6)	87.8 (50.2)
I/σ (last bin)[a]	25.9 (7.28)	24.9 (3.38)
R_{sym}[b] (last bin)[a]	0.058 (0.204)	0.062 (0.242)

[a] Last resolution bin is from 2.28 to 2.20 Å for the wild-type data and from 1.76 to 1.70 Å for the C13A−*p*NPP complex data. [b] $R_{sym} = \Sigma|(I_{hkl} - \langle I_{hkl}\rangle)|/\Sigma I_{hkl}$, where $\langle I_{hkl}\rangle$ is the average of I_{hkl} over all symmetry equivalents.

All data were indexed and integrated using the program DENZO (*38*), and merged and scaled together with the program SCALEPACK (*38*). The diffraction data for both mutant and wild-type crystals were indexed in space group $P2_12_12_1$. The data processing statistics are summarized in Table 1. Both data sets have similar unit cells, with two molecules in one asymmetric unit. The two molecules are termed molecule A and molecule B.

For the wild-type enzyme structure determination, the molecular replacement method (*39*) was used to obtain the initial phase information for the observed individual reflections, using the crystal structure of the bovine enzyme BPTP (PDB file 1pnt) as a search model (*30*). Because there is only a moderate degree of sequence identity between these two enzymes (39%), a polyalanine model of the BPTP structure (the backbone plus the β-carbon except for the glycine residues) was used to calculate the rotation and translation functions with the program AMoRe (*40*). The solution from this molecular replacement had a correlation coefficient of 0.416 and an *R* factor of 48.2%. The initial electron density map calculated using the solutions from AMoRe, at resolutions ranging from 8.0 to 2.8 Å, clearly showed the majority of the expected α-helices and β-strands. Density modification by the program DM (*41*) was carried out to improve the electron density map. The side chains (approximately 30%) with clearly defined electron density were built into the model using the program O (*42*), and the new model was then refined using XPLOR (*43*) with noncrystallographic symmetry constraints. The electron density maps, both $2F_o-F_c$ and F_o-F_c maps, were calculated from the refined model, and the model was rebuilt on the graphic display using the program O. This cycle was repeated with more and more side chains built into the model while the *R* factor improved. After the complete model had been built, it was refined with noncrystallographic symmetry restraints. The final R_{work} is 16.9%, with an R_{free} of 23.5% at resolution range of 12.0−2.2 Å (Table 2). There are 106 ordered water molecules in the structure, and two HEPES molecules each bound to the active site of a protein molecule. Figure 1A shows that HEPES has very well-defined electron density. The ϕ and ψ values of all the residues are in the allowed region of the Ramachandran plot, with more than 93% of the residues in the most favored regions.

Table 2: Structure Refinement Statistics

	wild type	C13A and *p*NPP
resolution range for refinement (Å)	12.0−2.2	12.0−1.7
total no. of protein atoms	2559	2592
average *B* factors of protein atoms (Å^2)	25	19
total no. of other molecules	106 water, 2 HEPES	368 water, 1 glycerol, 1 *p*NPP, 1 PO_4
average *B* factors of other molecules (Å^2)	31 (water), 35 (HEPES)	27 (water), 21 (glycerol), 17 (*p*NPP), 13 (PO_4)
rmsd for bond lengths (Å)	0.013	0.013
rmsd for bond angles (deg)	1.68	1.50
R_{free}[a]	0.235	0.215
R_{work}[a]	0.169	0.170

[a] $R = \Sigma(||F_{obs}| - k|F_{calc}||)/\Sigma|F_{obs}|$, where $|F_{obs}|$ and $|F_{calc}|$ are the absolute values of the observed and calculated structure factors, respectively, and k is the scale factor between the summation of the absolute values of the observed structure factors and that of the calculated structure factors. *R* factors were calculated using data in the resolution range shown for refinement without a σ cutoff. R_{free} was calculated with a set of data (7% for the wild-type data set and 8% for the C13A data) not used in the refinement. R_{work} was calculated against the data used in the refinement.

The refined model of wild-type LTP1 was used as a model for molecular replacement for the C13A mutant protein structure determination. A solution with positions for two molecules was found with a correlation coefficient of 0.776 and an *R* factor of 35.7%. Electron density maps that were calculated from this initial model showed clear density for the *p*NPP molecule at the active site of molecule A. However, no clear density for *p*NPP was seen in the active site of the other molecule (molecule B). Instead, density appropriate for a phosphate ion was seen. The model was refined using the program XPLOR with noncrystallographic symmetry restraints. There are 368 ordered water molecules, one *p*NPP molecule (Figure 1B), one phosphate ion, and one glycerol molecule found in the final model. The final R_{work} is 17.0%, and R_{free} is 21.5% at a resolution range of 12.0−1.7 Å (Table 2).

RESULTS AND DISCUSSION

Overall Structure of Wild-Type LTP1. The refined model of the wild-type LTP1 structure contains 156 amino acid residues for molecule A and 157 amino acid residues for molecule B. No electron density was seen for the first four residues at the amino terminus of molecule A, and for the first three residues of molecule B, presumably due to the high flexibility of the N-terminal residues. Because a mutant enzyme with 13 extra amino acids at the amino terminus derived from an N-terminal fusion with glutathione *S*-transferase exhibits virtually identical kinetic behavior compared to that of the wild-type protein, it is unlikely that the first few N-terminal residues serve an important role in catalysis (*15*).

The LTP1 structure has a fold similar to that found in the bovine and human enzymes (*30*, *32*). The enzyme consists of a twisted, central parallel β-sheet of four strands, with α-helices packed on either side (Figure 2). The secondary structure elements are shown in Figure 3, along with the sequence alignment with BPTP. The short helix α_3 in LTP1 is at the crystal packing interface, and is slightly different between molecule A and molecule B. There are two $\beta\alpha\beta$ motifs that form a Rossmann fold in the structure: $\beta_1\alpha_1\beta_2$ and $\beta_3\alpha_4\beta_4$. The active site is in the first $\beta\alpha\beta$ motif, with the sulfonate group of the substrate mimic HEPES binding at the N-terminal end of helix α_1 (Figure 2).

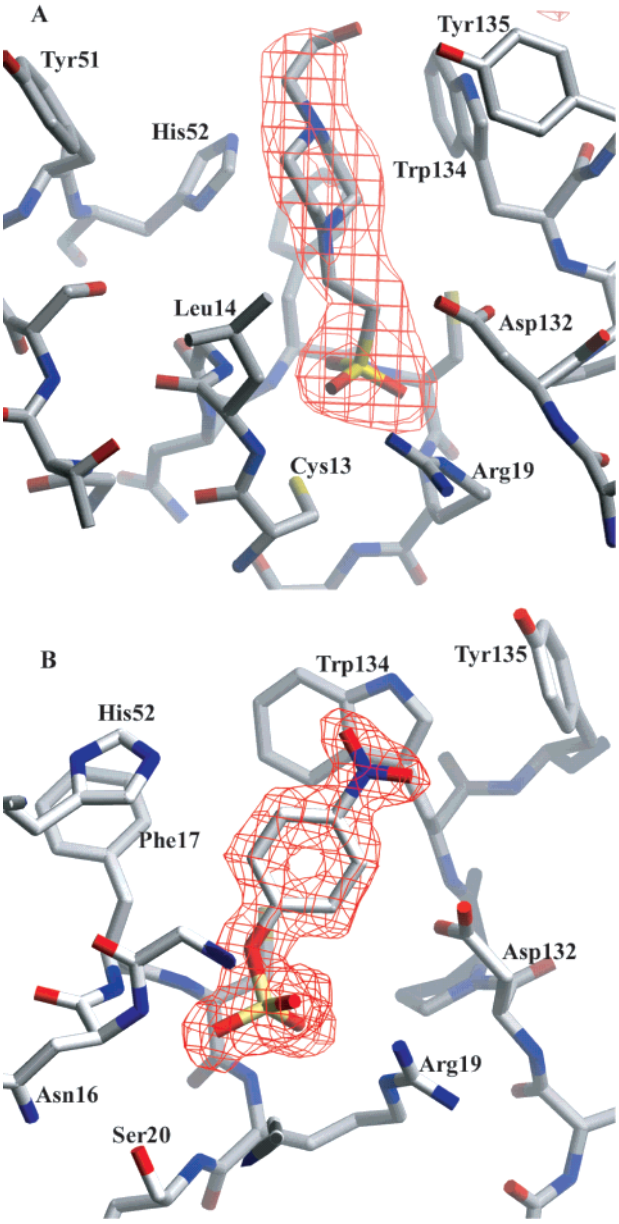

FIGURE 1: $F_o - F_c$ simulated annealed electron density omit maps showing the HEPES sulfonate molecule bound at the active site of molecule A in the wild-type LTP1 structure (A) and the electron density for the phosphate substrate *p*NPP in the mutant C13A complex with *p*NPP (B). The electron density in panel A was calculated with phases from the final model refined at 2.2 Å except that the HEPES molecules were omitted. The electron density in panel B was calculated with phases from the final model refined at 1.7 Å except that the *p*NPP molecule was omitted. For simulated annealing, a starting temperature of 1000 K and a cooling rate of 25 K per 50 steps were used. No harmonic restraints were imposed on the surrounding atoms. Both maps were calculated with a 5 Å cushion around the omitted molecules, and contoured at 3.0σ. These figures were generated with the program Setor (*46*).

The two molecules in the asymmetric unit are for the most part identical, with similar *B* factors for the corresponding residues. There is noncrystallographic 2-fold symmetry between the two molecules in the asymmetric unit, with the symmetry axis close to the active site on the surface where

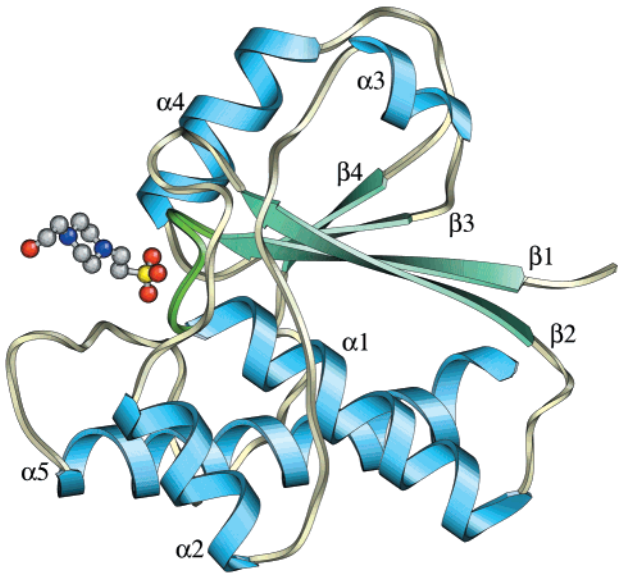

FIGURE 2: Ribbon diagram of the structure of the yeast low-molecular weight protein tyrosine phosphatase LTP1. The HEPES sulfonate molecule bound at the active site is shown as a ball-and-stick model. The consensus motif (P-loop) is between the C-terminal end of β_1 and the N-terminal end of α_1 (shown in green).

two molecules pack. The axis is almost perpendicular to helix α_4 (residues 95−104) and passes between the two Tyr-51 residues, which are on a loop between strand β_2 and helix α_2 and exhibit disordered side chains. The interaction between the two molecules on this packing interface includes a possible aromatic interaction between the two tyrosine rings, two symmetric H-bonds between the carbonyl oxygen of Asp-132 in one molecule and the Nϵ1 atom of Asn-99 in the other molecule and a hydrophobic interaction between the two Leu-14 side chains. In addition, there is an extensive water-mediated H-bonding network that appears to dominate the interface interactions. A total of 26 ordered water molecules were found at the dimer interface, with an average *B* factor of 25 Å^2, the same as that of the average protein atoms (25 Å^2). The buried surface of the noncrystallographic dimer in the crystals is about 750 Å^2 per monomer, including the surface areas of the active site cavities and that covered by water molecules that are in the interface of the dimer. The direct contact surface between the two protein molecules is about 450 Å^2 per monomer. The residues at the dimer interface are a mixture of hydrophobic and hydrophilic amino acids. However, this dimeric interaction does not appear to persist in solution as the enzyme was found to exist predominantly as a monomer in solution by gel filtration studies. The monomeric form of the enzyme has also been found to be the functional unit by pre-steady-state burst titration studies (*44*; H. Kirsch, C. Pokalsky, and R. L. Van Etten, unpublished results).

There is a tightly bound HEPES molecule in the active site of each protein molecule, with very well-defined density (Figure 1A). This is not surprising, because the crystals were grown from a 100 mM HEPES buffer at pH 7.0. Moreover, kinetic measurements confirmed that HEPES, which has a sulfonate group that mimics the phosphate group of the substrates, is a good competitive inhibitor of LTP1 at pH 7.0, with a K_i of 0.25 mM (Table 3). The atoms of the HEPES sulfonate group have very well-defined positions and have an average *B* factor of about 14 Å^2, similar to the *B* factors of the nearby protein atoms. This indicates that the HEPES molecule is at nearly full occupancy. The overall

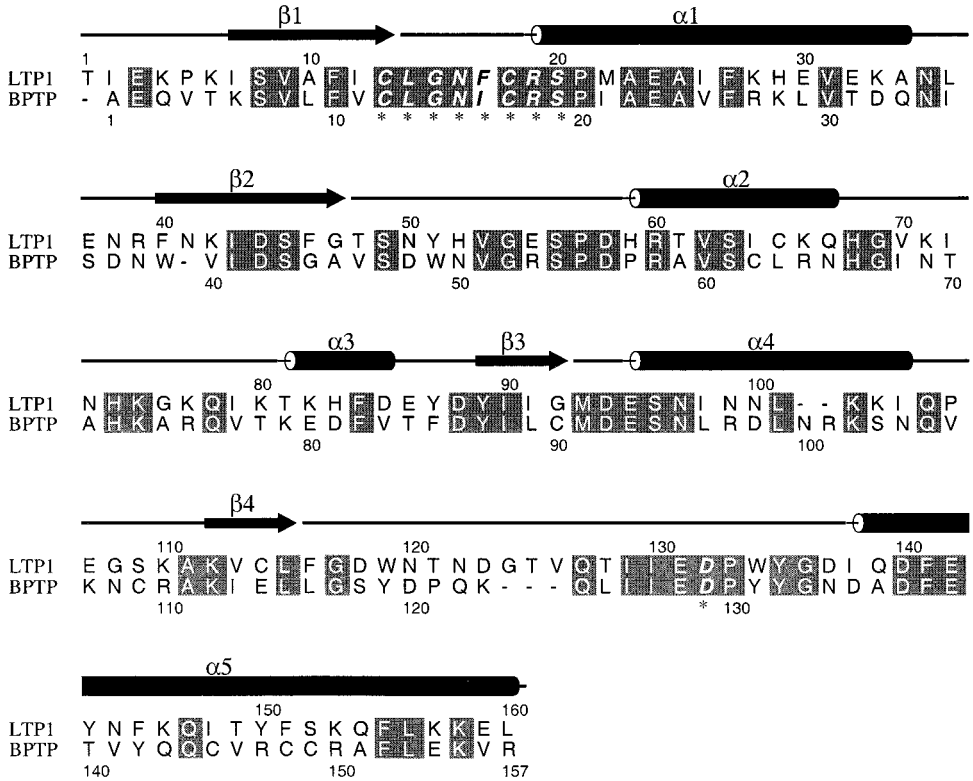

FIGURE 3: Sequence alignment of the low-molecular weight PTPases from yeast (LTP1) and bovine sources (BPTP). The sequences were aligned with the program Clustal-w, and the figure was generated with Alscript (*47*). Identical residues are highlighted in gray. The active site signature motif residues and the proton donor residue are indicated with asterisks. Above the sequences are shown the secondary structure elements of LTP1.

Table 3: Comparison of Kinetic and Inhibition Constants of LTP1 with Those of BPTP[a]

	Steady-State Kinetic Parameters[b]			
	LTP1		BPTP[c]	
	K_m	k_{cat}	K_m	k_{cat}
*p*NPP	0.017	1.24	0.38	34.2
phosphotyrosine	0.29	1.22	16.0	27.1
FMN	0.092	1.17		
β-naphthyl phosphate	0.58	1.47	1.20	29.5
α-naphthyl phosphate	4.6	0.33		
phenyl phosphate	0.046	1.01	3.60	27.5

	Inhibition Constants[d]			
	LTP1		BPTP[c]	
	pH	K_i	pH	K_i
vanadate	7.5	0.03	7.5	0.0054
molybdate	7.5	4.0	7.5	0.020
HEPES	5.0	4.0	5.0	5.3
HEPES	7.0	0.25	7.5	1.8

[a] K_m and K_i are given in units of millimolar, and k_{cat} is given in units of s^{-1}. [b] The steady-state kinetic parameters for BPTP were taken from Ostanin et al. (*15*) or Zhang et al. (*23*). The inhibition constants for BPTP were taken from Zhang et al. (*37*). [c] Kinetic measurements were taken in 100 mM NaOAc buffer (pH 5.0) and 1 mM EDTA at an ionic strength of 0.15 M, adjusted using NaCl. Reactions were carried out at 37 °C, and the rate of substrate dephosphorylation was established by measuring the rate of release of inorganic phosphate or *p*-nitrophenol. K_m and k_{cat} values were obtained by nonlinear curve fitting of the data to the Michaelis−Menten equation. [d] Inhibition constants were measured in 25 mM DEM buffer (pH 7.5), 100 mM NaOAc (pH 5.0), or 100 mM Bis-Tris (pH 7.0), with the ionic strength adjusted to 0.15 M using NaCl, and using *p*NPP as the substrate.

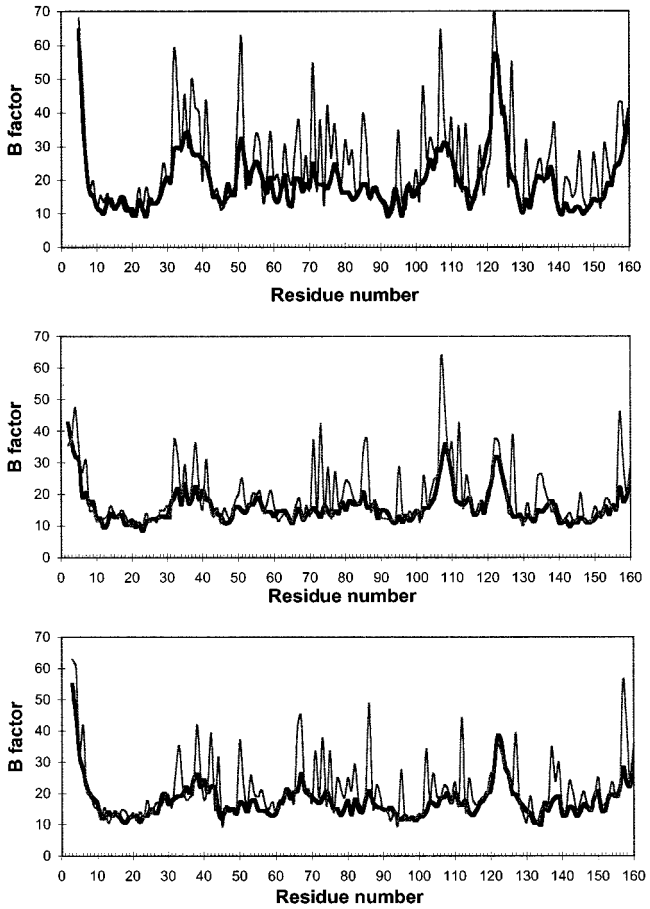

FIGURE 4: Temperature factor plots of wild-type LTP1 molecule A (top) and mutant C13A molecule A (middle) and molecule B (bottom). The thick black line depicts the average *B* factors for the main chain atoms. The thin gray line depicts the average *B* factors for the side chain atoms. The atoms of molecule B of wild-type LTP1 (not shown) have slightly higher temperature factors in some regions of the sequence, but in general follow a similar temperature factor pattern as those of molecule A. In both wild-type and mutant structures, the atoms of the active site signature sequence (residues 13−20) have the lowest *B* factors.

average *B* factor of protein atoms is about 25 Å^2, and that for the HEPES molecule is about 26 Å^2. Since HEPES and other sulfonates such as MES mimic the phosphate substrates binding to the P-loop, they were also found to cocrystallize with other PTPases, such as BPTP (*37*), HCPTPA (*32*), and VHR (*12*).

Structure of the Active Site. The important components of the active site consist of the phosphate-binding loop (P-loop, positions 13−20), an aspartic acid residue functioning as a proton donor to the leaving group of the substrate, and a group of hydrophobic residues that form the walls of the active site cavity. The active site cavity is deep, and the residues lining the walls of the cavity are mainly aromatic and hydrophobic residues, thus allowing for the favorable binding of the tyrosine ring of the substrate, as well as for substrate selectivity of the enzyme. The phosphate-binding loop is formed by the active site consensus sequence motif, which in LTP1 is CLGNFCRS as compared to CLGNICRS (different residue underlined) in its mammalian counterparts. This P-loop is the most ordered structure in the protein, and has low *B* factors for both main chain and side chain atoms (Figure 4). The P-loop conformation is stabilized by an extensive network of H-bonds in the three-dimensional structure. Some of these interactions are mediated by ordered water molecules that have *B* factors similar to those of nearby protein atoms. The backbone structure of the P-loop in this enzyme is effectively identical with that of other protein tyrosine phosphatases whose structures are known. The rmsd of Cα positions between the P-loops of LTP1 and BPTP is 0.17 Å, and that between the P-loops of BPTP and *Yersinia* PTPase is 0.37 Å (*6*). This indicates the importance of such a P-loop conformation for binding the phosphate group of the substrates effectively. One of the P-loop residues, Asn-16, is in a left-handed conformation. This residue forms a network of H-bonds with His-74, Ser-45, and Ser-20, and these interactions help to stabilize the overall structure of the phosphate-binding loop, allowing it to adopt the most favorable geometry for substrate binding. Residue Asn-16 is conserved among the low-M_r PTPases, and is in the same conformation in the other homologous structures (*30*, *32*). The residues of the P-loop are arranged such that all the amide protons between Cys-13 and Ser-20 face the center of the loop, where the sulfonate group of the HEPES molecule is bound (Figure 5A). The main chain NHs and Arg-19 side chain NHs participate in multiple, favorable hydrogen bonding interactions with each negatively charged sulfonate oxygen of the inhibitor (Table 4).

HEPES Binding Interactions. The binding of the competitive inhibitor HEPES shows that the interactions of the sulfonate group with the P-loop residues appear to contribute most of the binding energy of the HEPES molecule. The *B* factors of the atoms of HEPES increase progressively in moving from the sulfonate group to the distal CH_2OH group, with the hydroxyl oxygen having a *B* factor of >40 Å^2.

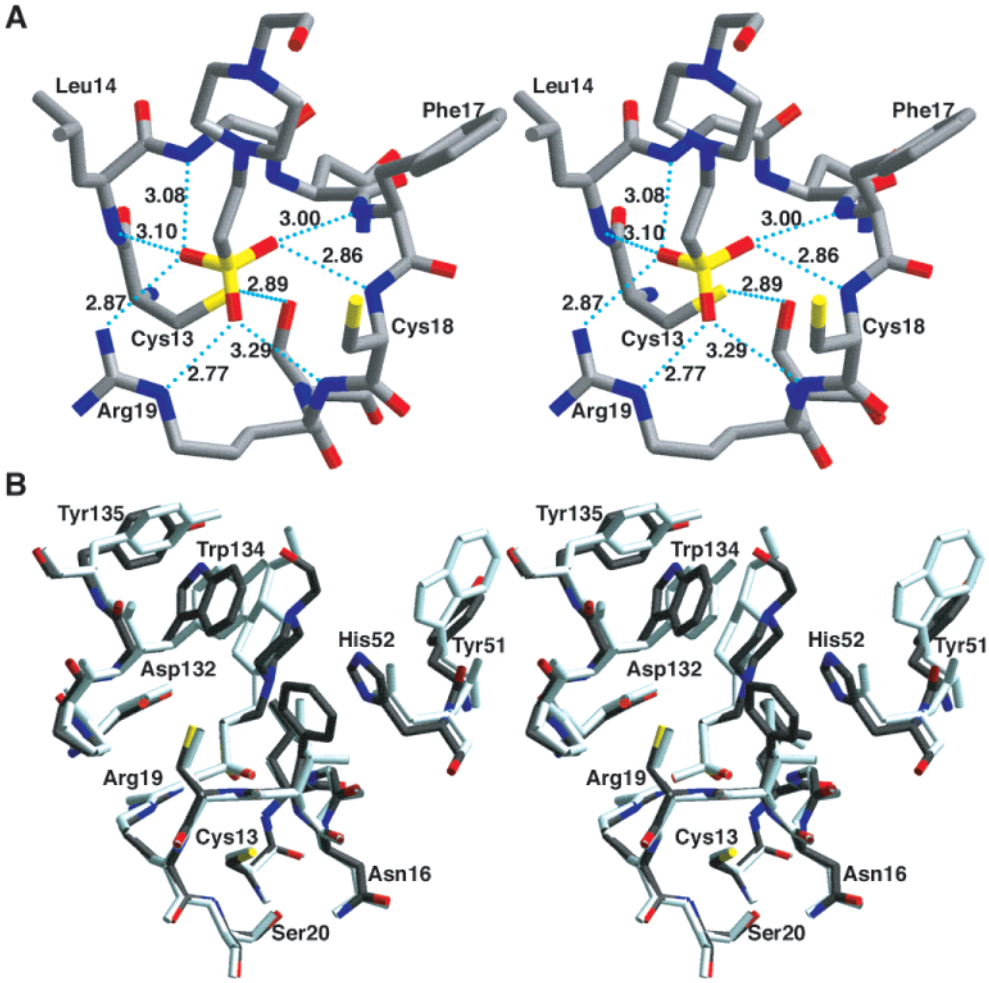

FIGURE 5: (A) Phosphate-binding loop (P-loop) structure of LTP1 with the bound HEPES molecule as a substrate analogue. All potential hydrogen bonds (<3.3 Å) between the HEPES sulfonate group and the P-loop residues are shown as dotted lines with distances given in angstroms. The P-loop is arranged such that all the NH groups between residues Cys-13 and Ser-20 are facing the center of the loop. The sulfonate oxygen atoms participate in H-bonds to the NH groups of the P-loop residues and to the side chain of Arg-19. The sulfonate group faces the side chain of nucleophilic Cys-13, with a distance between the sulfur atoms of ~3.77 Å. The side chain of Cys-13 forms an H-bond to the side chain of Ser-20. (B) The superposition of the active site residues of LTP1 and BPTP structures with bound HEPES. LTP1 is colored by elements, with black for the carbon atoms, while BPTP residues are shown in gray. The main chain atoms and most of the side chain atoms overlap very well. The HEPES sits in the active site, and is surrounded by aromatic and hydrophobic side chains. There are two more aromatic residues in the active site of LTP1, His-52 and Phe-17, on one wall of the active site cavity. The ring of HEPES tilts toward these two side chains in the LTP1 structure even though the sulfonate group occupies a position identical to that found in the BPTP complex.

Ring stacking and hydrophobic interactions also play a role in binding the HEPES molecule. The ring of the HEPES molecule is surrounded by side chains of residues His-52, Phe-17, Trp-134, and Leu-14. Compared to the active site of BPTP, there are two more aromatic residues on one wall in the active site of the LTP1 structure, Phe-17 and His-52 (Figure 5B). The side chains of these two residues are close to the ring of the HEPES molecule, and may also interact with the bound substrate. Although the sulfonate group of HEPES has identical binding interactions with the phosphate-binding loop in the structural superposition between LTP1 and BPTP, the piperazine ring of HEPES in the LTP1 structure tilts toward the side chains of residues Phe-17 and His-52. These additional aromatic residues in the active site of the LTP1 structure might help to explain kinetic differences among the low-M_r PTPases. The inhibition constants of HEPES were measured at two different pH values for LTP1 and BPTP (Table 3), and HEPES was found to be a better inhibitor for LTP1 than for BPTP. However, LTP1 exhibits markedly lower k_{cat} and smaller K_m values for all the substrates that were tested when compared to those of the bovine enzyme BPTP. For example, with *p*NPP as the substrate, the K_m for LTP1 is about 17 μM, while in the case of BPTP, it is about 380 μM at pH 5.0 (Table 3). On the basis of the HEPES complex structure presented here, it is reasonable to conclude that the aromatic interactions between the phenyl ring of *p*NPP and the side chains of His-52 and Phe-17 favor the binding of *p*NPP and similar substrates by LTP1 over the bovine homologue.

Arg-19 is a key residue for substrate binding. A mutation of Arg-18 in BPTP (equivalent to Arg-19 in LTP1) to an alanine completely inactivates the enzyme (*36*). The side chain of Arg-19 extends the backbone of the P-loop to form a complete circle surrounding the sulfonate moiety of HEPES (Figure 5A). Its guanidinium group forms strong H-bonds and salt bridges to the O1 and O3 atoms of the sulfonate

Table 4: Hydrogen Bonds between the Oxygen Atoms on the Phosphate or Sulfonate Group of the Bound Ligands and the Protein Atoms or Bound Water Molecules in both Mutant C13A and Wild-Type LTP1 Crystals[a]

	*p*NPP		PO_4		HEPES	
O1	G15 N	2.77	L14 N	2.89	L14 N	3.10
	L14 N	2.79	G15 N	2.82	G15 N	3.08
	R19 NH2	3.07	R19 NH2	3.08	R19 NH2	2.87
			w46	3.05		
O2	N16 N	2.94	N16 N	2.92	F17 N	3.00
	F17 N	2.99	F17 N	3.09	C18 N	2.86
			S20 Oγ	3.06		
O3	R19 Nϵ	2.81	R19 N	2.76	R19 Nϵ	2.77
	R19 N	2.79	R19 Nϵ	2.77	R19 N	3.29
O4	C18 N	2.99	F17 N	3.14		
			C18 N	2.87		
			w32	2.76		

[a] Each hydrogen bond is denoted by a protein atom or a water molecule, and the hydrogen bond distance is given in angstroms. The protein atoms are represented with the single-letter amino acid code with the residue number followed by the atom name. Water molecules are represented with a "w" followed by a number.

group (Table 4). Thus, the position of the guanidinium side chain is important in substrate binding, and is fixed by hydrogen bonding and charge interactions with the side chain of Asp-94 and the carbonyl oxygen of Ile-130 in the structure. In the case of BPTP, it is known that when Asp-92 (equivalent to Asp-94 in LTP1) is mutated to Ala, there is a 16-fold increase in K_m (*23*). The structure presented here shows the basis for this effect.

Catalytic Residues. The HEPES molecule bound at the active site mimics the initial binding of the substrate, with its sulfonate group facing the Sγ atom of the nucleophilic side chain of Cys-13 (Figure 5). The sulfur atom of Cys-13 is below the center of the three sulfonate oxygen atoms of HEPES. The distance between the sulfur atom of HEPES and the Sγ atom of Cys-13 is 3.77 Å, indicating that there is no direct interaction between these two atoms in this structure. Another critical catalytic residue in LTP1 is Asp-132, which is expected to donate a proton to the leaving group of the substrate in the enzyme reaction. When an equivalent aspartic acid residue in BPTP was mutated to an alanine, the enzyme exhibited a greater than 2000-fold reduction in V_{max} with *p*NPP as the substrate (*23*). Consistent with this, the carboxyl group of Asp-132 is close to the HEPES C1 atom (which corresponds to the phenolic oxygen of the phosphotyrosine), with its Oδ1 and Oδ2 atoms approximately 3.4 Å from the C1 atom of HEPES.

Crystal Structure of the C13A Mutant Complex with pNPP. To obtain further information relevant to understanding the enzyme mechanism and substrate specificity, we crystallized the catalytically inactive C13A mutant of LTP1 in a complex with the widely used artificial substrate *p*NPP. Crystals were obtained by cocrystallization with *p*NPP as described in Experimental Procedures. The mutant protein crystallized in a fashion similar to that of the wild-type protein, with two molecules in the asymmetric unit. In the refined model, there were 159 amino acid residues in one molecule (A), and 158 amino acid residues in the other molecule (B). No clear electron density was seen for the first residue of molecule A, or for the first two residues of molecule B. Molecule A has a *p*NPP molecule in the active site, while molecule B has a phosphate ion (see below for a discussion on the difference between the active sites of the two molecules).

The crystals of the C13A−*p*NPP complex were grown in the absence of glycerol, and glycerol was added later to a final concentration of 16% as a cryogenic solvent. Interestingly, a glycerol molecule from the cryosolvent is found at a crystal packing interface where three molecules make contact. This binding pocket is mainly hydrophobic, shallow, and with one side open to the bulk solvent channel. The glycerol molecule is surrounded by residues Gln-67, Glu-142, Ile-138, Glu-139, and Ile-64 of molecule A and residues Trp-134, Tyr-135, and Gly-136 and the side chain of Arg-60 of molecule B, and also residue Ile-104 from another molecule B. The side chains of Trp-134 and Tyr-135 of molecule B and the hydrophobic part of the side chain of Glu-142 and Gln-139 from molecule A form a hydrophobic circle near the bottom of the binding pocket. The side chains of Ile-64 and Ile-138 from molecule B and the side chain of Ile-104 from molecule A are on one side of the walls of the binding pocket. The O2 and O3 atoms of the glycerol molecule form two strong H-bonds to the Oϵ1 and Nϵ2 atoms of Gln-67 of molecule A. There are also three water-mediated H-bonds to the Oϵ1 atom of Gln-139, the NH1 atom of Arg-60, and the carbonyl oxygen atom of Trp-134. The pocket is large relative to the size of the glycerol molecule, with more than 10 ordered water molecules above the glycerol molecule.

Similar to that of the wild-type enzyme, the two molecules in the asymmetric unit of the C13A−*p*NPP crystal form a dimer with their active sites packed near each other, and with 2-fold noncrystallographic symmetry. However, the noncrystallographic symmetry is not perfect in the C13A−*p*NPP complex, with small differences at the dimer interface, and one protein molecule having a *p*NPP in the active site and the other having a phosphate ion.

The mutant protein crystal has a lower overall temperature factor (about 19 Å^2) than the wild-type protein crystals (about 25 Å^2), due to the lower temperature that was employed during data collection and possibly due to better packing (the mutant crystal diffracted to 1.7 Å, while the wild-type crystals diffracted only to 2.2 Å). The atoms in the helices and sheets have temperature factors similar to those in the wild-type crystal. However, the atoms in the loop regions are better defined than those in the wild-type crystal, and have lower temperature factors (Figure 4).

Interactions of pNPP with the Active Site Residues. Electron density maps showed clear density for a *p*NPP molecule at the active site of one of the molecules in the asymmetric unit (molecule A). The *p*NPP molecule is very well-ordered and at high occupancy (Figure 1B). Although its overall orientation in the active site is similar, the *p*NPP molecule binds more deeply in the active site as compared to the HEPES molecule in the wild-type structure (Figure 6; see also the comparison between the *p*NPP complex and the wild-type HEPES complex, below). The phosphate group therefore binds more deeply which allows more and stronger H-bonds to be formed between the P-loop and the phosphate group of *p*NPP (Table 4). The distance between the phosphorus atom of *p*NPP and the β-carbon of Ala-13 is 3.5 Å. Thus, the phosphate position of the *p*NPP is approximately at the phosphate position predicted for the phosphoenzyme intermediate, as shown in the BPTP−vanadate complex (*37*). The P-loop is therefore able to

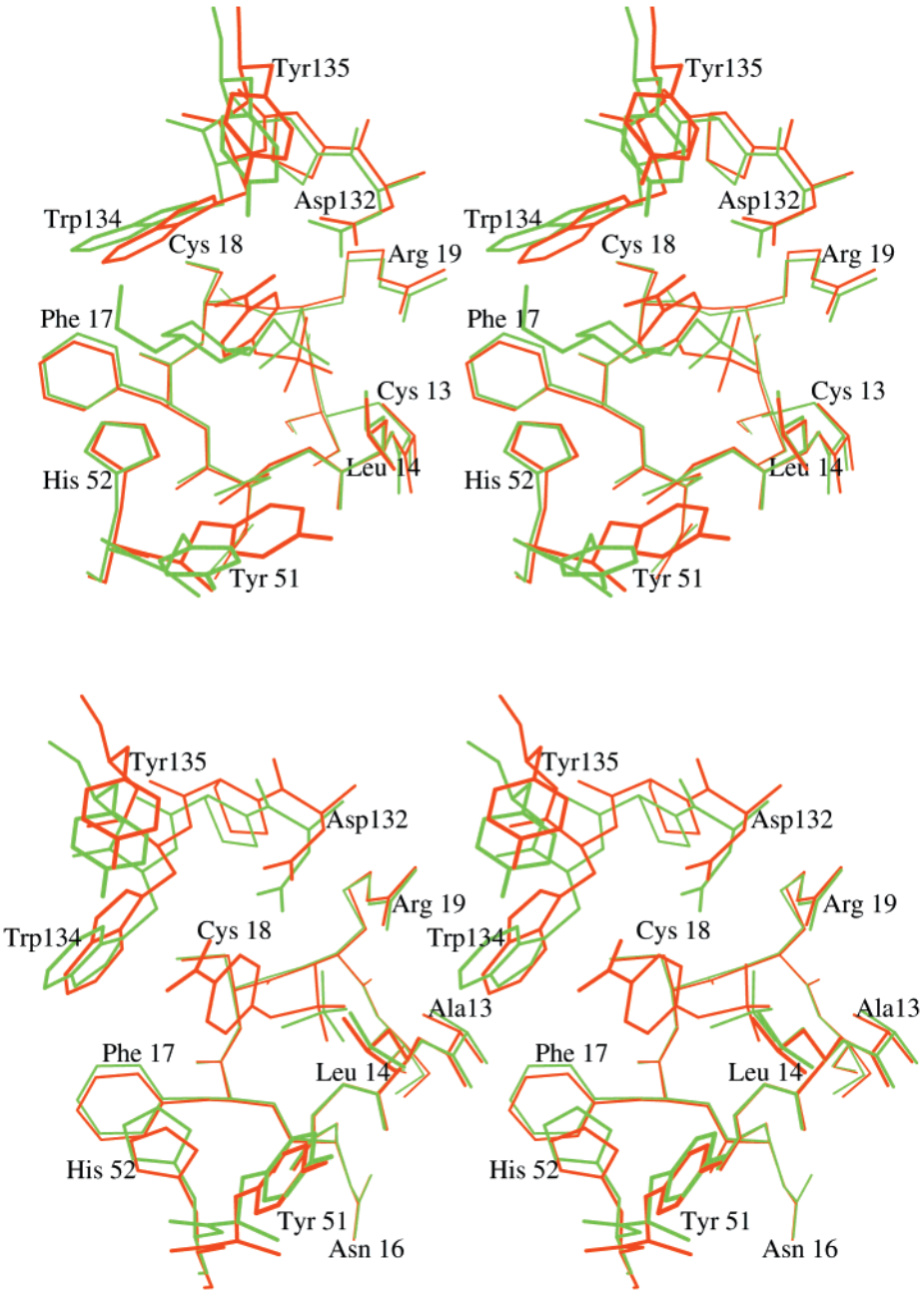

FIGURE 6: Stereoplots of the superposition of the active sites of the wild-type and C13A complex with *p*NPP (top panel) and the superposition of the two active sites of C13A complexes with *p*NPP and phosphate (bottom panel). In the top panel, the wild-type LTP1−HEPES complex is green and the C13A−*p*NPP complex is red. In the bottom panel, the C13A−PO_4 complex is green and the C13A−*p*NPP complex is red. The plots were generated with the program Molscript (*48*). In both cases, the P-loop atoms align very well, but residues lining the walls exhibit shifts in their positions. There are larger shifts for the residues on the walls between the C13A complex with *p*NPP and that with the phosphate ion, as compared to those between the C13A complex with *p*NPP and the wild-type protein with HEPES. The phosphate group of *p*NPP binds more deeply and closer to the position of the Cys-13 side chain than does the sulfonate group of HEPES in the wild-type protein (top). The phosphate ion also binds slightly deeper than the phosphate group of *p*NPP (bottom).

position the phosphate group close to the position occupied by Sγ of Cys-13 during the enzymatic reaction that leads to the formation of a phosphoenzyme intermediate. Similar to the HEPES molecule in the wild-type crystal, the phenyl ring of *p*NPP is surrounded by the side chains of His-52, Phe-17, Trp-134, and Leu-14. The side chain of residue Trp-134 is close to and stacks with the nitro group of *p*NPP, with the closest distance being about 3.26 Å. The tyrosyl side chain of Tyr-51 of molecule B (which is the nearby molecule in the crystal packing) stacks with that of Tyr-51 of molecule A, with its phenolic oxygen 3.4 Å from the O5 of the NO_2 group of *p*NPP.

The carboxyl group of Asp-132, the proton donor in the catalytic reaction, is also very close to the phenyl ring of *p*NPP, with its Oδ2 atom about 3.09 Å from C3 of *p*NPP. The Oδ1 atom H-bonds to the backbone nitrogen of residue Trp-134 with a distance of 3.00 Å. Residue Asp-132 donates a proton to the leaving group of the substrate, in this case the nitrophenol moiety, so it would be expected to be close to the leaving group oxygen of *p*NPP. The observation that it is instead close to the phenyl ring of *p*NPP is presumably an effect of the C13A mutation, which makes it possible for the *p*NPP molecule to move down, as described above.

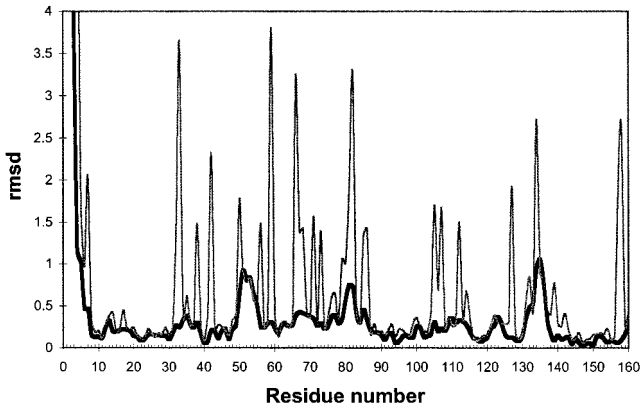

FIGURE 7: Root-mean-square deviation between the two molecules in the asymmetric unit present in the structure of C13A mutant in complex with *p*NPP and PO_4. The thick curve represents the rmsd between the main chain atoms. The thin curve represents the rmsd between the side chain atoms. The P-loop has an identical structure in the two molecules. The two largest peaks in the main chain curve correspond to residues 51 and 52, and 134 and 135, which are aromatic residues on the walls of the active site cavity that shift positions with different molecules bound in the active site. The peak around residues 81 and 82 is short helix α_3, which is in different crystal packing environments in the two molecules.

Comparison between the C13A Complexes of pNPP and PO_4. As mentioned above, the mutant C13A crystal has two molecules in the asymmetric unit, with one molecule (A) having a *p*NPP molecule in the active site and the other molecule (B) a phosphate ion. Figure 7 shows the rms deviation of the main chain and side chain atoms between molecule A and molecule B in the C13A−*p*NPP complex structure. The phosphate-binding loops (residues 13−20) have identical main chain conformations, with an rmsd for Cα atoms of 0.11 Å, and the side chains of the P-loop also have very similar positions (Figure 6). This is consistent with earlier conclusions that the structure of the P-loop is quite rigid (*37*). The positions of the two bound molecules are however slightly different. Compared to the phosphate group of *p*NPP, the inorganic phosphate ion binds slightly more deeply in the active site and is shifted (∼0.3 Å) toward residue Ser-20. The side chain of Ser-20 also moves toward the phosphate ion to form an H-bond between O2 of phosphate and Oγ of Ser-20 (Table 4). This brings it closer to Ala-13, which moves correspondingly to avoid contact. The shift of the phosphate ion allows it to form more H-bonds with the residues of the phosphate-binding loop, and thus to bind more tightly in the active site. In contrast, the *p*-nitrophenyl group interacts with the aromatic residues forming the wall of the active site cavity, and this tends to keep *p*NPP at a higher position compared to the phosphate ion.

The most striking structural differences between the two protein molecules can be seen in the positions of the aromatic residues that line the active site cavity walls (Figures 6 and 7). Residues in the loop containing residues Trp-134 and Tyr-135, as well as the proton donor Asp-132, show the largest movement, with shifts of the main chain atoms of more than 1 Å toward the center of active site cavity in molecule B (with a phosphate ion in the active site). The side chain of Trp-134 adopts a different conformation (rmsd > 2.5 Å) to avoid contact with the side chain of Phe-17 (Figure 6). The corresponding loop containing the proton donor aspartic acid in high-molecular weight PTPases also makes even larger movements and has been shown to be in an open conformation in the empty enzyme and to close upon substrate binding (*45*). Another loop with a large movement is the one containing residues Tyr-51 and His-52. The main chain coordinates for these residues in molecule B shift more than 0.8 Å toward the center of the active site cavity relative to those in molecule A. Consequently, the phosphate-bound molecule (molecule B) has a narrower active site cavity. The position in molecule B corresponding to that of the nitrophenyl moiety in molecule A has four ordered water molecules. Two of them H-bond to the carboxyl group of Asp-132 and the PO_4 group, and have low *B* factors. The other two bind weakly at the top of active site cavity, and have *B* factors of >30 Å^2.

Comparison of the pNPP Complex with the Wild-Type HEPES Complex. Comparison of molecule A (with *p*NPP in the active site) in the mutant C13A−*p*NPP crystal complex with the wild-type HEPES complex shows that the aromatic residues on the walls of the active site cavity have similar, but smaller, shifts, and the P-loop residues are almost identical. The main chain atoms of the P-loops of the *p*NPP complex and the wild-type HEPES complex superimpose almost perfectly (Figure 6), with an rmsd for Cα atoms of 0.14 Å. Moreover, even the side chains of the loop are in the same conformations. This again suggests the high rigidity of the P-loop.

In contrast, the residues on the walls of the active site cavity do exhibit some changes in relative positions. The loop containing Tyr-51 and His-52 shows a movement of about 0.5 Å. The largest movement occurs at residues Trp-134 and Tyr-135, where the main chain atoms shift about 0.8 Å. This is due to the interactions between *p*NPP and the side chains of Trp-134 and Asp-132. While the HEPES molecule is a relatively straight molecule, the *p*NPP molecule has a single bend at the phenolic oxygen. Therefore, when bound in the active site, the flat *p*-nitrophenyl group of *p*NPP is at a position slightly different from that of the (hydroxyethyl)piperazine portion of HEPES. The interactions of this *p*-nitrophenyl group with the side chains of Asp-132 and Trp-134 force the loop containing these residues to shift toward the surface of the protein relative to that in the wild-type HEPES complex. In the noncrystallographic dimer, this loop packs closely against the C-terminal end of helix α_4 of the other monomer. Therefore, the shift of the loop resulting from the binding of *p*NPP causes the other monomer to move away slightly. This is compensated in the crystal by the binding of inorganic phosphate in the active site of the other molecule, which allows the two molecules to move closer to each other. Therefore, the two protein molecules are able to stay close enough to form a dimer. As a result of the different movements in the two molecules that contain different ligands, the two monomers in the noncrystallographic dimer of the *p*NPP complex crystal are not exactly related by 2-fold symmetry, as compared to that in the crystal of the HEPES complex that has almost perfect 2-fold symmetry. Therefore, the two molecules in the *p*NPP complex crystal are not equivalent and can only pack as a complementary pair in the asymmetric unit. This results in a crystal in which one active site is exclusively occupied by *p*NPP and the other by inorganic phosphate.

The differences in the positions of these aromatic residues between the *p*NPP complex and the wild-type HEPES

complex are not as large as that between the *p*NPP complex and the phosphate complex, even though the *p*NPP complex and the phosphate complex are in the same crystal. This is because the *p*NPP molecule, with the *p*-nitrophenyl group, more closely resembles the extended HEPES molecule than a simple phosphate ion. Thus, the positions of the aromatic residues on the walls of the active site cavity vary with the bound ligand in the active site, indicating their importance in substrate binding and recognition.

The positions of the bound ligands, the *p*NPP molecule and the HEPES molecule, are different. This is due in part to two factors resulting from the mutation of Cys-13 to alanine in the mutant. The mutation allows more space for the phosphate group, and causes the elimination of the repulsive interaction between the negative charge on the phosphate group and the negative charge on the cysteine side chain (*23*, *27*, *29*; V. Dillet, R. L. Van Etten, and D. Bashford, unpublished results). On the basis of a structural superposition of the P-loops, the phosphate group in the *p*NPP complex is in a lower position relative to that of the sulfonate group in the HEPES complex. The phosphorus atom of *p*NPP moves down approximately 1.1 Å toward Ala-13 (which has replaced Cys-13 in the mutant), relative to the position of the sulfur atom of HEPES (in the wild-type structure). The O2 atom of *p*NPP tilts down to form two H-bonds to the amide NHs of residues 16 and 17 (Table 4). The bridging oxygen atom (O4) of the phosphate group is close to the position of the terminal oxygen atom O2 of HEPES, and forms one H-bond with the amide NH of residue Cys-18. The O2 atom of *p*NPP is within 1.7 Å of the position that would be occupied by the sulfur atom of Cys-13 of the wild-type protein. The binding mode of the phosphate group in the structure of the mutant complex with *p*NPP is closer to the binding mode of the phosphoenzyme intermediate, while the binding mode of the sulfonate group in the structure of the wild-type protein complex with HEPES is a better representation of the initial binding mode of the substrate. During the course of an enzymatic reaction leading to the formation of the phosphoenzyme intermediate, the formation of a bond between the phosphorus atom of the substrate and the cysteine sulfur of the enzyme brings the phosphate group more deeply into the active site. The structure of the P-loop favors the deep binding of phosphate, and thus facilitates the formation of the covalent phosphoenzyme intermediate.

In conclusion, the structure of LTP1 confirms the important roles of the aromatic residues lining the walls of the active site cavity in the enzymatic reaction. LTP1 has more aromatic residues on the walls of the active site cavity, which explains why this yeast enzyme has a higher affinity for typical apolar substrates and inhibitors compared to its mammalian counterparts. The substrate complex shows that the residues lining the walls of the active site cavity shift according to the bound ligand, indicating their dynamic nature and their importance in substrate binding and recognition. The structural results further confirm the critical role of the rigid P-loop in controlling the binding position of the phosphate group. The role of the P-loop is apparently not only to bind the phosphate moiety of the substrate but also to bring it into the proximity of the nucleophilic side chain of the cysteine, thus lowering the transition-state energy for formation of the phosphoenzyme intermediate.

REFERENCES

1. Nurse, P. (1990) *Nature 334*, 503−508.
2. Murray, A. W. (1992) *Nature 359*, 599−604.
3. Hunter, T. (1995) *Cell 80*, 225−236.
4. Streuli, M. (1996) *Curr. Opin. Cell Biol. 8*, 182−188.
5. Neel, B. G., and Tonks, N. K. (1997) *Curr. Opin. Cell Biol. 9*, 193−204.
6. Zhang, M., Stauffacher, C. V., and Van Etten, R. L. (1995) *Adv. Protein Phosphatases 9*, 1−23.
7. Stuckey, J. A., Schubert, H. L., Fauman, E. B., Zhang, Z.-Y., Dixon, J. E., and Saper, M. A. (1994) *Nature 370*, 571−575.
8. Barford, D., Flint, A. J., and Tonks, N. K. (1994) *Science 263*, 1397−1404.
9. Bilwes, A. M., Den Hertog, J., Hunter, T., and Noel, J. P. (1996) *Nature 382*, 555.
10. Hoffmann, K. M. V., Tonks, N. K., and Barford, D. (1997) *J. Biol. Chem. 272*, 27505.
11. Blenis, J. (1993) *Proc. Natl. Acad. Sci. U.S.A. 90*, 5889−5892.
12. Yuvaniyama, J., Denu, J. M., Dixon, J. E., and Saper, M. A. (1996) *Science 272*, 1328−1331.
13. Fauman, E. B., Cogswell, J. P., Lovejoy, B., Rocque, W. J., Holems, W., Montana, V. G., Piwnica-Worms, H., Rink, M. J., and Saper, M. A. (1998) *Cell 93*, 617−625.
14. Li, Y., and Strohl, W. R. (1996) *J. Bacteriol. 178*, 136−142.
15. Ostanin, K., Pokalsky, C., Wang, S., and Van Etten, R. L. (1995) *J. Biol. Chem. 270*, 18491−18499.
16. Manao, G., Pazzagli, L., Cirri, P., Casell, A., Camici, G., Cappugi, G., Saeed, A., and Ramponi, G. (1992) *J. Protein Chem. 11*, 333−345.
17. Waheed, A., Laidler, P. M., Wo, Y.-Y. P., and Van Etten, R. L. (1988) *Biochemistry 27*, 4265−4273.
18. Wo, Y.-Y. P., McCormack, A. L., Shabanowitz, J., Hunt, D. F., Davis, J. P., Mitchell, G. L., and Van Etten, R. L. (1992) *J. Biol. Chem. 267*, 10856−10865.
19. Wo, Y.-Y. P., Zhou, M.-M., Stevis, P., Davis, J. P., Zhang, Z.-Y., and Van Etten, R. L. (1992) *Biochemistry 31*, 1712−1721.
20. Modesti, A., Cirri, P., Raugei, F., Carraresi, L., Magherini, F., Manao, G., Camici, G., and Ramponi, G. (1995) *FEBS Lett. 375*, 235−238.
21. Stein, E., Lane, A. A., Cerretti, D. P., Shoecklnann, H. O., Schroff, A. D., Van Etten, R. L., and Daniel, T. O. (1998) *Genes Dev. 12*, 667−678.
22. Mondesert, O., Moreno, S., and Russell, P. (1994) *J. Biol. Chem. 269*, 27996−27999.
23. Zhang, Z., Harms, E., and Van Etten, R. L. (1994) *J. Biol. Chem. 269*, 25947−25950.
24. Zhang, Z.-Y., and Dixon, J. E. (1993) *Biochemistry 32*, 9340−9345.
25. Lohse, D. L., Denu, J. M., Santoro, N., and Dixon, J. E. (1997) *Biochemistry 36*, 4568−4575.
26. Denu, J. M., Zhou, G., Guo, Y., and Dixon, J. E. (1995) *Biochemistry 34*, 3396−3403.
27. Evans, B., Tishmack, P. A., Pokalsky, C., Zhang, M., and Van Etten, R. L. (1996) *Biochemistry 35*, 13609−13617.
28. Tabernero, L., Evans, B., Tishmack, P. A., Van Etten, R. L., and Stauffacher, C. V. (1999) *Biochemistry 38*, 11651−11658.
29. Peters, G. H., Frimurer, T. M., and Olsen, O. H. (1998) *Biochemistry 37*, 5383−5393.
30. Zhang, M., Van Etten, R. L., and Stauffacher, C. V. (1994) *Biochemistry 33*, 11097.
31. Su, X.-D., Taddei, N., Stefani, M., Ramponi, G., and Nordlund, P. (1994) *Nature 370*, 575−578.
32. Zhang, M., Stauffacher, C. V., Lin, D., and Van Etten, R. L. (1998) *J. Biol. Chem. 273*, 21714−21720.
33. Logan, T. M., Zhou, M.-M., Nettesheim, D. F., Meadows, R. P., Van Etten, R. L., and Fesik, S. W. (1994) *Biochemistry 33*, 11087−11096.
34. Vandeyar, M. A., Weiner, M. P., Hutton, C. J., and Batt, C. A. (1988) *Gene 65*, 129.
35. Baykov, A. A., Evtushenko, O. A., and Avaeva, S. N. (1988) *Anal. Biochem. 171*, 266−270.
36. Davis, J. P., Zhou, M.-M., and Van Etten, R. L. (1994) *J. Biol. Chem. 269*, 8734−8740.

37. Zhang, M., Zhou, M., Van Etten, R. L., and Stauffacher, C. V. (1997) *Biochemistry 36*, 15−23.
38. Otwinowski, A. (1993) *DENZO, Data Collection and Processing*, pp 56−62, Daresbury Laboratory, Warrington, U.K.
39. Rossmann, M. G., and Blow, D. M. (1962) *Acta Crystallogr. 15*, 24−31.
40. Navaza, J. (1987) *Acta Crystallogr. A43*, 645−653.
41. Cowtan, K. (1994) *Joint CCP4 and ESF-EACBM Newsletter on Protein Crystallography 31*, 34−38.
42. Jones, T. A., Zou, J. Y., Cowan, S. W., and Kjeldgaard, M. (1991) *Acta Crystallogr. A47*, 110−119.
43. Brunger, A. T., Kuriyan, J., and Karplus, M. (1987) *Science 235*, 458−460.
44. Zhang, Z.-Y., and Van Etten, R. L. (1991) *J. Biol. Chem. 266*, 1516−1525.
45. Jia, Z. (1997) *Biochem. Cell Biol. 75*, 17−26.
46. Evans, S. V. (1993) *J. Mol. Graphics 11*, 134−138.
47. Barton, G. J. (1993) *Protein Eng. 6*, 37−40.
48. Kraulis, P. J. (1991) *J. Appl. Crystallogr. 24*, 946−950.

BI991348D